

Letters to *Analytical Chemistry*

## Monolithic Silicon Chip for Immunofluorescence Detection on Single Magnetic Beads

Emile P. Dupont,<sup>\*,†</sup> Estelle Labonne,<sup>‡,§</sup> Caroline Vandevyver,<sup>||</sup> Ulrike Lehmann,<sup>†,⊥</sup> Edoardo Charbon,<sup>‡,⊗</sup> and Martin A. M. Gijs<sup>†</sup>

Laboratory of Microsystems, School of Computer and Communication Sciences, and Research Commission EPFL-SNF, Ecole Polytechnique Fédérale de Lausanne (EPFL), CH-1015 Lausanne, Switzerland

While fluorescence detection is widely used for bioassays owing to its high sensitivity, a complete fluorescent microscopy setup, comprised of a light source, optical filters, a microscope body, and a camera, still is bulky equipment, compromising its use in a point-of-care environment. Here we propose an integrated monolithic silicon chip for integrated magnetic manipulation and optical detection of fluorescently labeled magnetic beads. Our approach permits microscopeless measurement of the fluorescence of a single microparticle. We demonstrate the viability of this approach by the detection of cancer biomarker 5D10 monoclonal antibodies (mAbs) in a noncompetitive sandwich immunoassay performed on the surface of magnetic beads, in a phosphate buffered saline–bovine serum albumin (PBS–BSA) solution, with a detection limit of 1 ng mL<sup>-1</sup>.

A microtiter plate-based enzyme-linked immunosorbent assay (ELISA) exploits the sensitivity and specificity of the interaction between a target antigen (Ag), its specific capture antibody (Ab), and detection Ab to form a traceable sandwich immunocomplex. Such a test typically takes a few hours and is based on either colorimetric or fluorescent detection principles. Miniaturized microchannel-based bioanalysis systems offer the advantage of strong analysis time reduction, while consuming only minute quantities of samples and reagents (typically a few microliters).<sup>1–4</sup> Moreover, the use in such systems of micro- or nanoparticles (“beads”) that can be functionalized using a wide range of available surface chemistries prevents the need for functionalization of the micro-

channels.<sup>5–9</sup> Magnetic beads, in addition, can be easily magnetically actuated and recovered, explaining why they are increasingly employed as a solid support in bioanalysis.<sup>10–14</sup> Several quantitative magnetic bead-based immunoassays using optical or fluorescent detection have been presented in a miniaturized format.<sup>15–17</sup> In all of these approaches, the use of a high-end (fluorescent) microscope detection platform was key for achieving a good system performance and high detection sensitivity. Few examples of successful integration of optical detection and microfluidics can be found in the literature. On-chip optical imaging was demonstrated by Heng et al.<sup>18</sup> through the use of CCD sensors underneath a microfluidic channel. Fluorescence detection was achieved on-chip by Balslev et al.,<sup>19</sup> integrating a laser source, waveguides, and photodiodes in a microsystem. However, complete integration of optoelectronics and microfluidics in the same disposable device may not be the most cost-effective option.<sup>20</sup>

We report here a complementary metal-oxide-semiconductor (CMOS) chip for detecting in a microfluidic channel fluorescent immunocomplexes located on the surface of magnetic beads. Our approach is not based on a fluorescence microscope detection platform but on the measurement of photon-induced electrical current

\* To whom correspondence should be addressed. E. P. Dupont, Laboratory of Microsystems, Ecole Polytechnique Fédérale de Lausanne (EPFL), STI-LMIS2-BM3135-Station 17, CH-1015 Lausanne (Switzerland). Fax: (+41)216935950. E-mail: emile.dupont@epfl.ch.

<sup>†</sup> Laboratory of Microsystems.

<sup>‡</sup> School of Computer and Communication Sciences.

<sup>§</sup> Current address: CEA-LETI, 38054 Grenoble, France.

<sup>||</sup> Research Commission EPFL-SNF.

<sup>⊥</sup> Current address: Microsens SA, 2002 Neuchâtel, Switzerland.

<sup>⊗</sup> Current address: Circuits and Systems Group, Faculty of EEMCS, Delft University of Technology, Delft, The Netherlands.

(1) Auroux, P. A.; Iossifidis, D.; Reyes, D. R.; Manz, A. *Anal. Chem.* **2002**, *74*, 2637–2652.

(2) Li, D. *Encyclopedia of Microfluidics and Nanofluidics*; Springer: New York, 2008.

(3) Vilkner, T.; Janasek, D.; Manz, A. *Anal. Chem.* **2004**, *76*, 3373–3385.

(4) West, J.; Becker, M.; Tombrink, S.; Manz, A. *Anal. Chem.* **2008**, *80*, 4403–4419.

(5) Haes, A. J.; Terray, A.; Collins, G. E. *Anal. Chem.* **2006**, *78*, 8412–8420.

(6) Hong, J. W.; Studer, V.; Hang, G.; Anderson, W. F.; Quake, S. R. *Nat. Biotechnol.* **2004**, *22*, 435–439.

(7) Kurita, R.; Yokota, Y.; Sato, Y.; Mizutani, F.; Niwa, O. *Anal. Chem.* **2006**, *78*, 5525–5531.

(8) Lim, C. T.; Zhang, Y. *Biosens. Bioelectron.* **2007**, *22*, 1197–1204.

(9) Verpoorte, E. *Lab Chip* **2003**, *3*, 60N–68N.

(10) Doyle, P. S.; Bibette, J.; Bancaud, A.; Viovy, J. L. *Science* **2002**, *295*, 2237–2237.

(11) Dreyfus, R.; Baudry, J.; Roper, M. L.; Fermigier, M.; Stone, H. A.; Bibette, J. *Nature* **2005**, *437*, 862–865.

(12) Gijs, M. A. M. *Microfluid. Nanofluid.* **2004**, *1*, 22–40.

(13) Lehmann, U.; Hadjidi, S.; Parashar, V. K.; Vandevyver, C.; Rida, A.; Gijs, M. A. M. *Sens. Actuators, B: Chem.* **2006**, *117*, 457–463.

(14) Pamme, N. *Lab Chip* **2006**, *6*, 24–38.

(15) Choi, J. W.; Oh, K. W.; Thomas, J. H.; Heineman, W. R.; Halsall, H. B.; Nevin, J. H.; Helmicki, A. J.; Henderson, H. T.; Ahn, C. H. *Lab Chip* **2002**, *2*, 27–30.

(16) Kim, K. S.; Park, J. K. *Lab Chip* **2005**, *5*, 657–664.

(17) Lacharme, F.; Vandevyver, C.; Gijs, M. A. M. *Anal. Chem.* **2008**, *80*, 2905–2910.

(18) Heng, X.; Erickson, D.; Baugh, L. R.; Yaqoob, Z.; Sternberg, P. W.; Psaltis, D.; Yang, C. H. *Lab Chip* **2006**, *6*, 1274–1276.

(19) Balslev, S.; Jorgensen, A. M.; Bilenberg, B.; Mogensen, K. B.; Snakenborg, D.; Geschke, O.; Kutter, J. P.; Kristensen, A. *Lab Chip* **2006**, *6*, 213–217.

(20) Myers, F. B.; Lee, L. P. *Lab Chip* **2008**, *8*, 2015–2031.

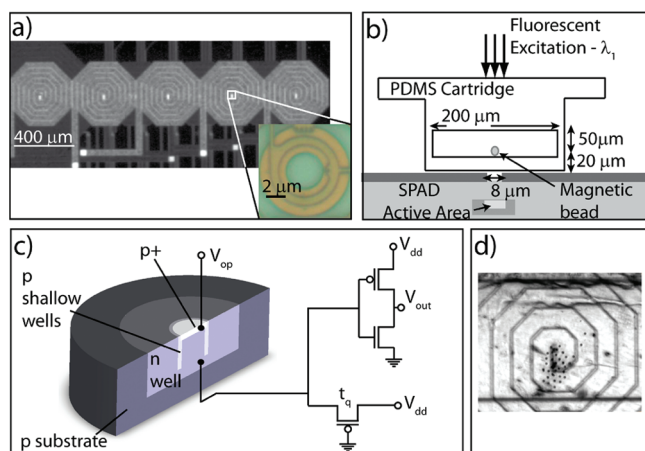


**Figure 1.** (a) Micrograph of the CMOS chip, showing the top layer of octagonal microcoils. Insert: zoom on one of the SPAD detectors in the center of a microcoil. (b) Cross-section view of the chip with the superposed PDMS microfluidic cartridge with an indication of the dimensions. (c) Schematic view and scheme of the SPAD structure with its electrical control circuit. (d) Applying current in a microcoil causes an attractive magnetic force to the nearby magnetic beads, whereby a single magnetic bead is positioned over the SPAD active area.

pulses in single photon avalanche diodes (SPADs)<sup>21</sup> integrated in the center of magnetic actuation microcoils on a silicon chip (see Figure 1a,b) (see Supporting Information, CMOS chip design and fabrication). We profit from the advantageous signal-to-noise ratio and integration properties of a SPAD, which is a p–n junction reverse biased above the breakdown voltage  $V_{bd}$  by an excess bias voltage  $V_e = V_{dd} - V_{bd}$ . The electrical configuration, schematically shown in Figure 1c, causes the optical gain to become virtually infinite, thus making single photon detection possible. When a photon is absorbed in the multiplication region, a set of avalanche current pulses is triggered, the integration of which forms the SPAD output signal.

Fluorescent immunocomplexes are formed on streptavidin-coated magnetic beads by first incubating the latter off-chip with biotinylated polyclonal rabbit antimouse immunoglobulin (IgG) for providing the capture Ab (see Supporting Information, Immunoassay protocol). As target Ag, we use either a commercial mouse IgG mAb in varying concentrations (0.25–5000 ng/mL) or a 5D10 murine mAb solution obtained from a hybridoma cell culture medium (see Supporting Information, 5D10 mAb production). A polyclonal goat Cy3-conjugated antimouse IgG is used as the fluorescent detection Ab. After injection of the bead–immunocomplex solution in a low-cost, disposable polydimethylsiloxane (PDMS) microfluidic channel (see Supporting Information, Microfluidic cartridge fabrication), the beads are transported using time-dependent current actuation of the microcoil array, allowing precise positioning of single beads over a SPAD. To achieve this, the chip and microfluidic channel are first put in a constant magnetic field generated by a 4 cm diameter external copper coil. Before the microcoil's current is switched on, the beads are at arbitrary positions in the microchannel. When applying a current through a microcoil, we can obtain an attractive or repulsive force on the beads, depending if the microcoil-induced magnetic field is in the same or opposite sense of the field generated

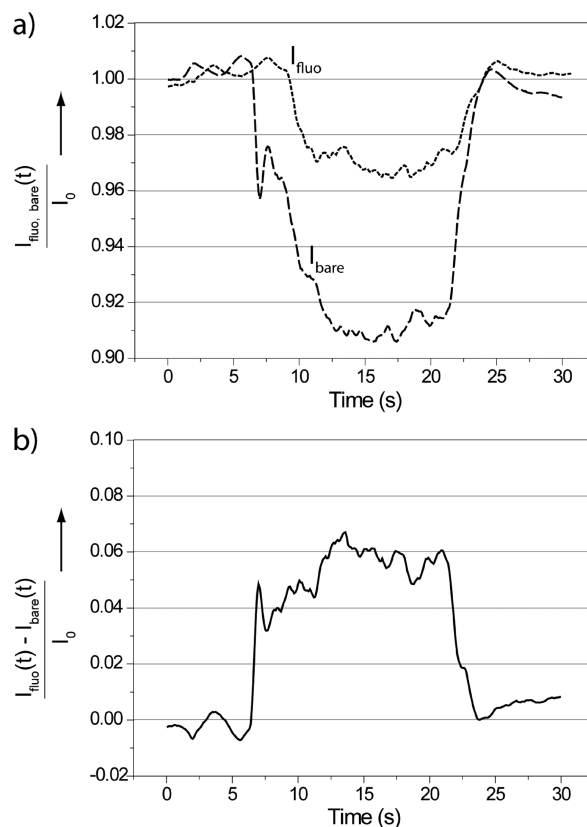


**Figure 2.** Normalized photocurrents detected by translation in the PDMS microchannel of a magnetic bead over the SPAD active area.  $I_0$  is the SPAD output when no bead is above the detector. Signals in part a are for a nonfluorescent bare bead ( $I_{bare}$ ) and a fluorescent bead ( $I_{fluo}$ ). The fluorescent beads are prepared by a first incubation with the capture Ab, then with a 5 ng/mL mouse IgG target Ag solution, and finally with Cy3-conjugated antimouse IgG fluorescent detection Ab. The normalized differential signal in part b represents the extra-counted photons originating from the presence of fluorescent molecules on the bead surface.

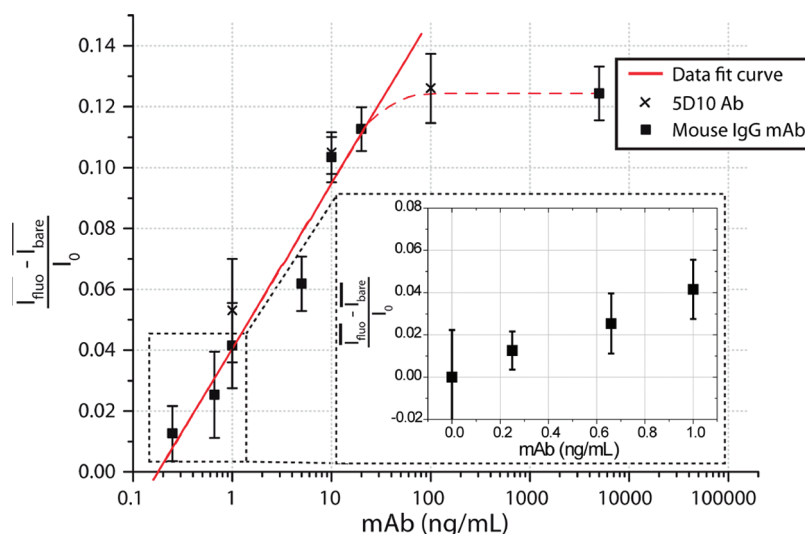
by the external coil, respectively. Figure 1d shows magnetic beads attracted to the center of the coil. Using the combined actuation of adjacent coils, we are able to isolate a single bead and position it over a SPAD; interference due to the presence of other beads is thereby avoided. We then measure the fluorescent signal due to a single stationary bead on top of the SPAD.

Figure 2a shows examples of the normalized photocurrent detected by the SPAD when examining the translation in the microchannel of a nonfluorescent bare bead and a bead functionalized by applying first 5 ng/mL mouse IgG as target Ag, followed by exposure to the fluorescent detection Ab solution. When the magnetic bead is not fluorescently labeled, its presence above the SPAD is detected by its shadow, as in a microeclipse effect, resulting in a ~9% reduced photocurrent.<sup>22</sup> In the case of the fluorescent bead, the SPAD registers an additional photon count, caused by the fluorescent aura around the bead (see further), and the decrease in photon count during transition is lower. Figure 2b is the differential curve obtained using the two curves of Figure 2a and represents the extra-counted photons originating from the presence of fluorescent detection Ab.

Figure 3 is a graph of the normalized time-averaged fluorescent response of the SPAD detection system to different target Ag

(21) Niclass, C.; Rochas, A.; Besse, P. A.; Charbon, E. *IEEE J. Solid-State Circuits* **2005**, *9*, 1847–1854.

(22) Lehmann, U.; Sergio, M.; Pietrolola, S.; Dupont, E.; Niclass, C.; Gijis, M. A. M.; Charbon, E. *Sens. Actuators, B: Chem.* **2008**, *132*, 411–417.



**Figure 3.** Average normalized differential signal due to a single magnetic bead positioned over the SPAD active area for different target Ag concentrations.  $I_0$  is the SPAD output when no bead is above the detector.  $I_{\text{fluo}}$  is the time-averaged signal when a fluorescent magnetic bead is positioned over the SPAD active area, while  $I_{\text{bare}}$  is the time-averaged signal corresponding to the presence of a bare bead. The ■ and × represent the data using either mouse IgG mAb or 5D10 mAb as target Ag, respectively. The data points and error bars correspond to the average and variance of 4–6 measurements performed on nominally identical single beads, respectively. The dashed curve is a guide to the eye, while the full curve is a logarithmic fit (correlation coefficient:  $R = 0.976$ ). The inset details the fluorescence at low concentrations on a linear concentration scale.

concentrations. The data points correspond to the fluorescent intensity of single magnetic beads positioned over a SPAD. We combine here the results obtained using as target Ag both the mouse IgG mAb (■) and the 5D10 mAb (×). The graph shows that our system has a sensitive range of around 3 decades of concentration, which is a typical value for fluorescent detection using synthetic dyes like Cy3.<sup>23</sup> When the analyte concentration is higher than 10 ng/mL, we observe saturation of the bead surface with target Ag. The inset of Figure 3 shows the data points for the lowest concentrations on a linear concentration scale. The first point corresponds to the SPAD output obtained when using 0 ng/mL target Ag but after performing the complete immunoassay protocol. The point coincides with the fluorescent response of a bare magnetic bead, indicating a negligible aspecific adsorption of the fluorescent detection Abs on the bead surface. We estimate that the detection limit of our system is around 1 ng/mL, the fluorescence response at lower concentrations being influenced by statistical bead-to-bead variations. This limit is comparable to the one achieved by performing a similar sandwich immunoassay on beads using a (normal) fluorescent microscope setup.<sup>17</sup>

We also could correlate the SPAD detection signal to the presence of a fluorescent layer on the surface on a magnetic bead, observed as a fluorescent “aura” using an inverted microscope setup (Zeiss Axio Observer.A1 with Hal 100 light-source). In these experiments, the Cy3 dye is excited at  $\lambda_1 = 550$  nm. Parts a and c of Figure 4 show the fluorescence intensity profiles and corresponding images of magnetic beads obtained with a 32× objective, (a) without and (c) with application of a fluorescent emission filter ( $\lambda_2 = 605$  nm) placed between the particle and the microscope detection objective. Curves i represent the intensity profile for a bare bead, while curves ii correspond to the intensity profile of a fluorescently labeled bead. Curves iii of parts b and d of Figure 4 represent each the intensity difference between the curves i and ii of parts a and c of Figure

4, respectively. The curves iii confirm essentially that a photocurrent increase can be associated with the presence of fluorescent molecules on the bead surface. The bead images inserted at the right in Figure 4a,c confirm that these extra photons can be perceived by the microscope as originating from a fluorescent aura around the magnetic bead indeed.

Moreover, we simulated in two dimensions the experimental diffraction data using the finite element method (FEM) in COMSOL Multiphysics. The FEM simulation model applies Kirchhoff’s approximation to the problem, in which the scalar complex amplitude of the wave field is determined by solving the Helmholtz equation (eq 1) (where  $k_0 = 2\pi/\lambda_i$  is the wavenumber determined by the wavelength  $\lambda_i$  of the coherent light source) with appropriate boundary conditions.

$$\Delta u(x, y) + k_0^2 u(x, y) = 0 \quad (1)$$

Solving the Helmholtz equation by numerical methods and using the Kirchhoff’s approximation are widely used approaches to model electromagnetic waves propagation in dielectric media, when considering monochromatic light.<sup>24,25</sup> In our first model (Figure 4e), we simulate a bare bead (without fluorescent labels) observed by the microscope. In the second simulation (Figure 4g), we model a fluorescent bead, when observed through the  $\lambda_2$  filter. Further details are reported in the Supporting Information, Finite Element Method. Parts f and h of Figure 4 show the agreement between the simulations and the experimental observations, without and with the use of the emission filter, respectively. The squares correspond to the experimental curve i in Figure 4a and curve ii in Figure 4c, respectively, and the full lines are simulated curves, as obtained along the dashed line segments in

(24) Gross, H.; Model, R.; Bär, M.; Wurm, M.; Bodermann, B.; Rathsfeld, A. *Measurement* **2006**, 39, 782–794.

(25) Testorf, M. E.; Fiddy, M. A. *Opt. Commun.* **2000**, 176, 365–372.

(23) Rick, W. *Luminescence* **2003**, 18, 25–30.

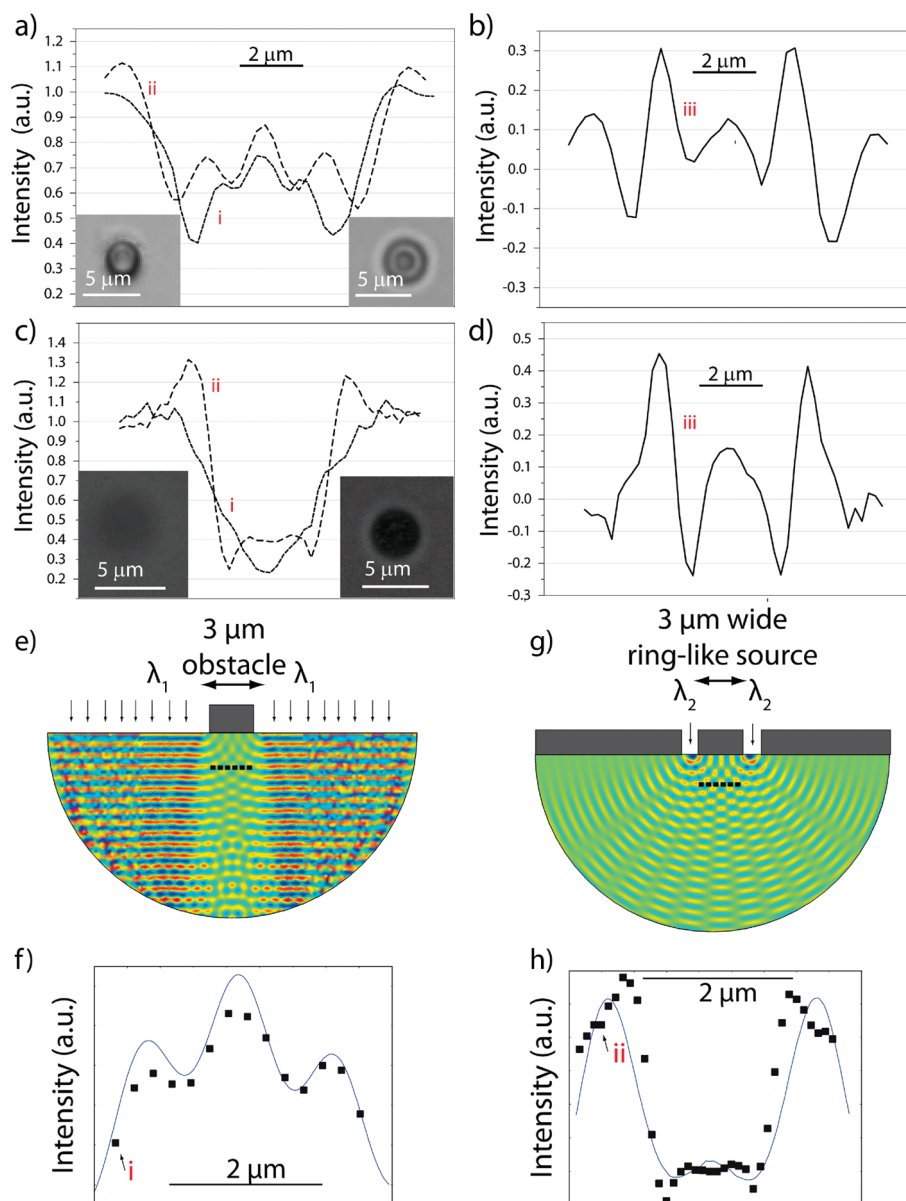


**Figure 4.** (a–d) Fluorescence intensity profiles and images of magnetic beads measured using an inverted microscope setup (32× objective) and (e–h) two-dimensional finite element simulations of light diffraction. Experimental data are taken (a, b) without and (c, d) with the use of a fluorescent emission filter ( $\lambda_2 = 605$  nm) placed between the bead and the microscope detection objective; the role of the filter is to remove the fluorescent excitation signal at  $\lambda_1 = 550$  nm. In parts a and c, curves i and ii are the intensity profiles corresponding to a bare and fluorescent bead, respectively. The left and right insert show the microscopic images of a bare bead and a fluorescent bead (for a target Ag concentration of 1 mg/mL), respectively. Curve iii in parts b and d is obtained by subtracting curve ii from curve i for the data of parts a and c, respectively. Parts e and g show the FEM simulations corresponding to the experimental data of parts a and c, respectively. In parts f and h, the ■ correspond to the experimental curve i of part a and ii of part c, respectively, while the full lines are the simulated curves along the dashed line segment in parts e and g, respectively.

parts e and g of Figure 4, respectively. The good agreement between experiments and simulations demonstrates that our FEM model correctly represents the experimental situation.

In conclusion, we reported an integrated monolithic CMOS chip for sensitive fluorescent detection of immunocomplexes (down to 1 ng/mL of target Ag concentration) on the surface of single magnetic beads. The latter are transported in a PDMS microchannel by current-actuation of microcoils, allowing precise positioning of single beads over a SPAD. Finally, we elucidated the auralike origin of the additional photons detected by the SPAD when fluorescent molecules are present on the magnetic bead surface. We anticipate that our integrated magnetic bead manipulation and detection chip can be combined with a variety of

available magnetic bead surface chemistries, offering high flexibility and great potential to our approach for a large number of sensitive bioassays and will be of interest especially for miniaturized portable applications that involve sensitive fluorescent detection.

#### SUPPORTING INFORMATION AVAILABLE

Additional information as noted in text. This material is available free of charge via the Internet at <http://pubs.acs.org>.

Received for review October 5, 2009. Accepted October 30, 2009.

AC902241J